A hierarchical framework for estimating neuroretinal rim area using 3D spectral domain optical coherence tomography (SD-OCT) optic nerve head (ONH) images of healthy and glaucoma eyes

Akram Belghith*,[1], Christopher Bowd[1], Robert N. Weinreb[1] and Linda M. Zangwill[1]

Abstract— **Glaucoma is a chronic neurodegenerative disease characterized by loss of retinal ganglion cells, resulting in distinctive changes in the optic nerve head (ONH) and retinal nerve fiber layer (RNFL). Important advances in technology for non-invasive imaging of the eye have been made providing quantitative tools to measure structural changes in ONH topography, a crucial step in diagnosing and monitoring glaucoma. 3D spectral domain optical coherence tomography (SD-OCT), an optical imaging technique, has been commonly used to discriminate glaucomatous from healthy subjects. In this paper, we present a new approach for locating the Bruch's membrane opening BMO and then estimating the optic disc size and rim area of 3D Spectralis SD-OCT images. To deal with the overlapping of the Bruch's membrane BM layer and the border tissue of Elschnig due to the poor image resolution, we propose the use of image deconvolution approach to separate these layers. To estimate the optic disc size and rim area, we propose the use of a new regression method based on the artificial neural network principal component analysis (ANN-PCA), which allows us to model irregularity in the BMO estimation due to scan shifts and/or poor image quality. The diagnostic accuracy of rim area, and rim to disc area ratio is compared to the diagnostic accuracy of global RNFL thickness measurements provided by two commercially available SD-OCT devices using receiver operating characteristic curve analyses.**

Index Terms— **Glaucoma, rim area, SD-OCT, deconvolution, Artificial Neural Network Principal component analysis**

I. Introduction

Glaucoma is an optic neuropathy in which the eye's internal pressure increases and contributes to nerve fiber damage in the optic nerve. The increase in intraocular pressure (IOP) is generally due to either a malformation or a malfunction of the eye's drainage system [1]. Initially asymptomatic for several years, the glaucoma develops gradually and painlessly. Elevated IOP is the strongest risk factor leading to the loss of peripheral vision and, in an advanced state, irreversible blindness. However, early detection and treatment can slow, or even halt the progression of the disease. Hence, it is important to develop clinical routines for progression detection in order to avoid permanent damage to the optic nerve head.

Since Hermann von Helmholtz invented the ophthalmoscope in 1851, physicians were able to examine the disc clinically and identify damages in the optic nerve head associated with glaucoma. This requires identification of the outer and inner borders of the neuroretinal rim and visual estimation of the amount of rim tissue. However, the inner and the outer borders of the ONH neural tissue are not always visible by clinical examination techniques [2]. Furthermore, the clinical examination of the ONH remains subjective, qualitative and variably reproducible [3].

Advances in optical coherence tomography (OCT) have provided a noninvasive optical imaging technique that has been used to evaluate structural changes in the ONH and particularly the rim area. Recently, spectral domain OCT (SD OCT) advances have brought a significant improvement in image capture speed and resolution and exhibit some of the characteristics of a good diagnostic tool such as high sensitivity and specificity, good reproducibility, ability to detect change over time, simplicity in usage and interpretation and convenience for both patient and physician [4].

Several studies have proposed the Bruch's membrane opening (BMO) (i.e; the termination of the Bruch's membrane (BM) layer) as a reference point from which rim parameters of the ONH can be computed [5]. Hence, rim area quantification requires the identification of the BMO (the inner border) and the internal limiting membrane (ILM) (the outer border).

Many advances have been made to identify different ONH layers. In [6], authors proposed a diffusion filtering methodology to denoise and to detect the layers instead of the traditional image thresholding. However, the edge information could be lost in the denoised images which limits the use of the method particularly when the layers overlap. In [7], authors used multi-scale 3-D graph search for segmenting the optic nerve head. As a cost function, the gradient magnitude of the dark-to-bright and bright-to-dark transitions from top to bottom of the OCT volume was calculated. This technique was used also in [8]. While the estimation of the ILM is easy to perform (the border of the ONH tissue), the estimation of the layers highly depends on the accuracy of the estimated gradient-based dark-to-bright and bright-to-dark transitions which can be a major drawback for poor quality and noisy images, particularly in the BM area. Due to these limitations, physicians still commonly rely on manual segmentation of ONH structures [2], [5] which is a time-consuming process that is impractical for routine clinical use.

A challenge in BMO identification is how to determine whether the algorithm is correctly identifying the BMO,

[1] Hamilton Glaucoma Center, University of California San Diego, La Jolla, California. * Corresponding author: abelghith@ucsd.edu. The authors acknowledge the funding and support of the National Eye Institute (grant numbers: U10EY14267, EY019869, EY021818, EY022039 and EY08208, EY11008, P30EY022589 and EY13959)

978-1-4244-7929-0/14/$26.00

and is able to differentiate between the BM layer and the border tissue of Elschnig. This is particularly challenging when there is an overlapping of these structures (and others) due to the poor image resolution. Moreover, a poor signal to noise ratio can affect the accuracy of BMO identification result when the noise is not taken into account within the identification scheme.

In this paper, we propose a new segmentation algorithm for the identification of the for BM segmentation and BMO identification:

1) In contrast to [6], and in order to develop a noise robust algorithm, we propose the consideration of the BMO segmentation problem as a missing data problem where we jointly estimate the noise hyper-parameters and the segmented image. To deal with the overlapping of the BM and the border tissue of Elschnig layers due to the poor image resolution, we propose the use of an image deconvolution approach [9] which consists of assigning to each layer a specific shape (or filter) and then estimate its hyper-parameters.
2) To overcome the problem of presence of gaps and/or lack of good quality scans, we propose the use of a new regression method to estimate the optic disc size and rim area. In fact, in the segments of the ONH with poor quality, the BMO points are considered as inaccurate data and the available BMO points in the good quality segments of the ONH are then mainly used to estimate the inaccurate BMO. In order to inject the connected shape aspect of the BMO (i.e. the elliptical aspect) in our regression algorithm, we propose the use of the artificial neural network principal component analysis (ANN-PCA) [10], which allows us to properly model such aspect.

The remainder of this paper is divided into three sections. In section II, the proposed BM layer segmentation is presented. We describe in section III the BMO regression scheme to estimate the optic disc size and rim area. Then, in section IV, results obtained by applying the proposed scheme to real data are presented. The rim area measurements using the current approach were compared to those from the built-in software of Cirrus HD-OCT (Optic disc Cube 200x200, Cirrus OCT). The diagnostic accuracy of rim area, and rim to disc area ratio also was compared to the diagnostic accuracy of global RNFL thickness measurements provided by two commercially available SD-OCT devices using receiver operating characteristic curve analyses.

II. Bruch's membrane layer segmentation

In this work, we consider 3D Spectralis SD-OCT images (Heidelberg Engineering) radial scan images. Each 3D image consists of 48 enhanced depth imaging radial 2D B-scans centered on the optic nerve head (c.f. Fig.1). We denote by Y_k a given B-scan, $k = 1 : 48$. Each B-scan (M x N) consists of several inter-retinal layers (e.g; the BM layer, the Retinal Nerve Fiber layer (RNFL),...). We assume that every layer to be segmented follows a Gamma distribution and extends across the entire width of the image. Because the inter-retinal layers have different thicknesses, each layer can be defined by a curve modeling its skeleton and a filter or set of filters modeling its thickness. We denote by X_k the image containing the skeletons of different inter-retinal layers, the relation between $Y_k = y_k(i,j)$ $i = 1...M$, $j = 1...N$ and $X_k = x_k(i,j)$ can be expressed as a convolution product:

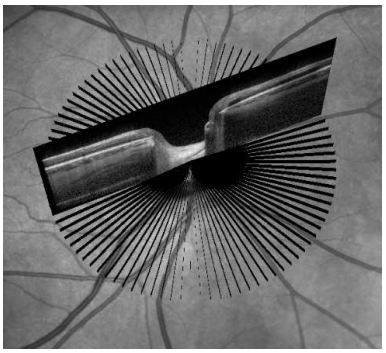

Fig. 1. 3D Spectralis SD-OCT images (Heidelberg Engineering) radial scan.

$$y_k(i,j) = (a_k(i,j).x_k(i,j)) * h(i,j) + b_k(i,j). \quad (1)$$

where $*$ is the convolution operator, $h(i,j)$ are the filters modeling the thickness of the layer at (i,j), $A_k = a_k(i,j)$ $i = 1...M$, $j = 1...N$ is the image intensity of the layer at (i,j) and $B_k = b_k(i,j)$ is white additive Gaussian noise with standard deviation σ. To segment the different layers, it is sufficient to estimate their skeletons X_k and the hyper-parameters of the filters $h(i,j)$. In this paper, we are only interested in the segmentation of the BM layer. The direct model is then expressed as:

$$y_k(i,j) = (a_k(i,j).x_k(i,j)) * h(i,j) + r_k(i,j). \quad (2)$$

where $x_k(i,j) = 1$ if the the pixel at (i,j) belongs to the skeleton of BM, otherwise $x_k(i,j) = 0$, and $r_k(i,j)$ consists of the additive noise $b(i,j)$ and the rest of the other layers. For simplicity's sake, we will assume that the filters $h(i,j)$ are Gaussian with the same hyper-parameter. In order to build connected skeletons, we considered an object-oriented approach rather than the pixel-oriented approach [11]. Therefore, short segments (20 pixels in our case) are added to or deleted from the current configuration depending on their state (connected or not). Note that shorter segments have been considered in the termination of the skeletons for a better estimation accuracy. The estimation of the model parameter and hyperparameters are addressed using a Monte Carlo Markov Chain [12].

III. Optic disc size estimation

Once we estimated separately the BMO points in each image of the 48 B-scans, we consider the whole 3D volume to estimate the optic disc size and then the rim area. In [13], [14], authors manually selected the BMO and then used a simple spline method to derive a closed curve representing the BMO around the ONH. However, this method is not

adapted to our scheme because the BMO were automatically estimated and therefore, we need a more sophisticated approach to overcome the problem of gaps presence due the blood vessels and/or lack of good quality scans.
Hence, our aim is 1) to properly integrate the elliptical shape of the BMO curve and 2) to only rely on the reliable BMO points in the estimation scheme. Note that our aim is not to fit an ellipse to the data but to use the elliptical shape as prior shape to estimate the curve that best represent the data. An elegant way to address this task is to use the inverse artificial neural network ANN-PCA to model the elliptical shape of the BMO curve. The ANN-PCA [15] has proved its high accuracy to model the non-linear PC in many field such as the electroencephalography signal [16] and metabolism [17]. The proposed method was inspired from [10] where authors adapt the network to the case of circular curve and missing data. We extended this work to the case of elliptical curve and unreliable data. The proposed network is presented in Fig. 2. The output $\hat{y_i}$ depends on the observation y_i, the input x_i and the network weights $W = \{W_1, W_2, W_3\}$. In order to obtain a elliptical constraint, the couple (z_1, z_2) (Fig. 2) are constrained to lie on an ellipse $(z_1^2)/a^2 + (z_2^2)/b^2 = 1$ where a, b are the hyper-parameters of the ellipse and $z_1 = w_1(1,1).x_1 + w_1(2,1).x_2$ and $z_2 = w_1(1,2).x_1 + w_1(2,2).x_2$. The aim is then to estimate the function $\Phi_{gen}(.)$ which generates $\hat{y_k}$ by minimizing the error function depending on W, (a, b) and $z = (z_1, z_2)$:

$$E(w, x, a, b) = \sum_{k}^{K} ||\hat{y}_k - y_k||^2 \tag{3}$$

where $\hat{y}_k = W_3.f(W_2.z)$ and f is an activation function. This error function can be minimized using the gradient optimization algorithm [18] and the derivation of the network weights W are obtained by standard back propagation [19]. As one can see, all the estimated BMO points equally contribute to the error function E. In order to penalize the unreliable BMO points (e.g; the BMO points belonging to noisy scans), we propose to modify the error function (Eq. 3) by assigning to each BMO point a new hyperparameter $0 \leq \alpha_k \leq 1$ modeling its accuracy:

$$E(w, x, a, b) = \sum_{k}^{K} \alpha_k ||\hat{y}_k - y_k||^2 \tag{4}$$

The more the BMO estimation is accurate, the more α_k is close to 1. In this work, we used the signal to noise ratio SNR parameters of each B-scan to set α_k: $\alpha_k = 0.1$ if SNR< 10, $\alpha_k = 0.5$ if SNR< 20 and $\alpha_k = 1$ otherwise. By this way, the error introduced by an inaccurate BMO point is penalized and it partially contributes to the gradient. Note that when the segmentation algorithm fails to identify the BMO in a given scan, α_k is set to 0 (missing data case).

IV. Experiments

In this section, we first assess the proposed BMO identification scheme. Then, we compare the obtained rim area measurements using this approach to those from built-in software of Cirrus HD-OCT. Finally, the diagnostic accuracy of the estimated rim area and rim to disc area ratio using the SD-OCT images was also compared to diagnostic accuracy of 1) global RNFL thickness measurements provided by two commercially available SD-OCT devices (Cirrus HD-OCT and Spectralis SD-OCT) and 2) the rim area and rim to disc area ratio provided by Cirrus HD-OCT.

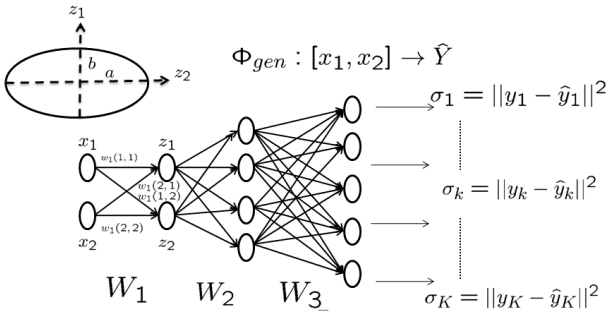

Fig. 2. A standard MLP network with elliptical associative topology. This network is composed of 3 parts [1-1-2]. The first two layers aim at modeling the elliptical constraint (the bottleneck layer). The last two layers aim at reconstructing the data to $\hat{y_i}$ thanks to Φ_{gen} function.

The proposed framework was experimentally validated with real datasets. Eligible participants were recruited from the University of California, San Diego (UCSD) Diagnostic Innovations in Glaucoma Study (DIGS). The glaucoma diagnostic accuracy (area under receiver operating characteristic (AUROC)) was estimated using 105 glaucoma and 100 healthy eyes.

In order to evaluate the BMO segmentation scheme, an expert manually identified the BMO on 80 B-scans (one vertical (12:00 to 6:00 o'clock position) and one horizontal (9:00 to 3:00 o'clock position) of 20 normal and 20 glaucomatous eyes). The automated segmentation failure rate (the number of B-scans where neither of the two BMO positions was segmented) ranged from 0 to 2, by definition (0 when the mean difference < 3 pixels, 1 when the mean difference < 5 pixels and 2 when the mean difference > 5 pixels). In 74 B-scans (92.5%), the failure rate was 0, in 5 B-scans (6.25%), the failure rate was 1 and in 1 B-scans (1.25%), the failure rate was 2.

Fig. 3 presents an example of BM segmentation result using the proposed method and the recently described multi-scale 3-D graph search method [7]. As one can see, the graph method confounds the border tissue of Elschnig with the BM layer which is not the case with the proposed method. Note that because no other dedicated BMO segmentation algorithm is available, no comparison to other methods on the same dataset was conducted in this paper. However, we have compared the BMO-based disc area and rim area estimated with the proposed approach using Spectralis EDI radial scans to those from built-in software of Cirrus SDOCT device. The coefficient of determination r^2 between the two devices for the BMO-based disc area was $r^2 = 0.845$ (p-value <0.001) and for the rim area was $r^2 = 0.783$ (p-value <0.001).

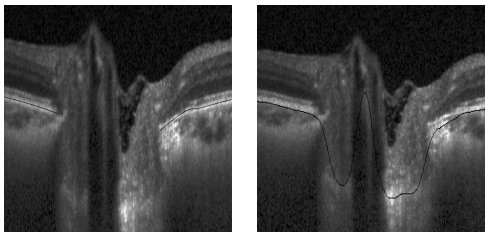

(a) (b)

Fig. 3. (a) BM segmentation using the proposed method, (b) BM segmentation using [7]

Feature(s)	Spectralis (95%CI)	Cirrus * (95%CI)
Global RNFL thickness*	0.918 (0.85-0.96)	0.908 (0.81-0.94)
Rim Area**	0.87 (0.75-0.94)	0.82 (0.71-0.91)
Rim to Disc Ratio**	0.81 (0.69-0.89)	0.75 (0.62-0.84)
Rim area ** and RNFL thickness*	**0.935 (0.87-0.98)**	0.913 (0.84-0.96)

TABLE I

GLAUCOMA DIAGNOSTIC ACCURACY (AREA UNDER RECEIVER OPERATING CHARACTERISTIC CURVE (AUROC)) WITH 95% CONFIDENCE INTERVAL. * MEASUREMENTS PROVIDED BY THE BUILT-IN SOFTWARES OF SPECTRALIS AND CIRRUS SD-OCT DEVICES AND ** MEASUREMENTS OBTAINED BY THE PRESENT METHOD.

The diagnostic accuracy of rim area, and rim to disc area ratio were compared to Retinal Nerve Fiber Layer (RNFL) thickness measurements and the combination of rim area and RNFL thickness for glaucoma detection. We used STATA SE software (Stata Corporation, College Station, TX, USA) to estimate the area under receiver operating characteristic curve using the bootstrap method [21]. Results are presented in Tab. I. The diagnostic accuracy of RNFL thickness tended to be better than rim area and rim to disc ratio but varied by instrument. The combination of the RNFL thickness and the rim area led to the best diagnostic accuracy.

V. CONCLUSION

In this paper, a new method for Bruch's membrane layer segmentation has been proposed. We particularly focus on the formulation of the segmentation problem as a missing data problem. The task of estimating the optic disc size and then the rim area is tackled with an inverse artificial neural network ANN-PCA approach to model the elliptical shape of the BMO curve and to deal with inaccurate BMO estimation. The validation of the proposed approach with real data has shown high correlation with the expert manual segmentation and the built-in software of Cirrus SDOCT device measurements. AUROC results suggest that the combination of the RNFL thickness and the rim area measurements is a good choice for discriminating between glaucoma and healthy eyes.

REFERENCES

[1] I. Dielemans, PT De Jong, R. Stolk, J.R. Vingerling, D.E. Grobbee, A. Hofman, et al., "Primary open-angle glaucoma, intraocular pressure, and diabetes mellitus in the general elderly population. the rotterdam study.," *Ophthalmology*, vol. 103, no. 8, pp. 1271, 1996.

[2] Alexandre SC Reis, Glen P Sharpe, Hongli Yang, Marcelo T Nicolela, Claude F Burgoyne, and Balwantray C Chauhan, "Optic disc margin anatomy in patients with glaucoma and normal controls with spectral domain optical coherence tomography," *Ophthalmology*, vol. 119, no. 4, pp. 738–747, 2012.

[3] G.J. Jaffe and J. Caprioli, "Optical coherence tomography to detect and manage retinal disease and glaucoma," *American journal of ophthalmology*, vol. 137, no. 1, pp. 156–169, 2004.

[4] T C Chen, B Cense, M.C Pierce, N Nassif, B.H Park, S.H Yun, B.R White, B.E Bouma, G.J Tearney, and J.F de Boer, "Spectral domain optical coherence tomography: ultra-high speed, ultra-high resolution ophthalmic imaging," *Archives of Ophthalmology*, vol. 123, no. 12, pp. 1715, 2005.

[5] Alexandre SC Reis, Neil O'Leary, Hongli Yang, Glen P Sharpe, Marcelo T Nicolela, Claude F Burgoyne, and Balwantray C Chauhan, "Influence of clinically invisible, but optical coherence tomography detected, optic disc margin anatomy on neuroretinal rim evaluation," *Investigative ophthalmology & visual science*, vol. 53, no. 4, pp. 1852–1860, 2012.

[6] Delia Cabrera Fernández, Harry M Salinas, and Carmen A Puliafito, "Automated detection of retinal layer structures on optical coherence tomography images," *Optics Express*, vol. 13, no. 25, pp. 10200–10216, 2005.

[7] Kyungmoo Lee, Meindert Niemeijer, Mona K Garvin, Young H Kwon, Milan Sonka, and Michael D Abràmoff, "Segmentation of the optic disc in 3-d oct scans of the optic nerve head," *Medical Imaging, IEEE Transactions on*, vol. 29, no. 1, pp. 159–168, 2010.

[8] Alexander Ehnes, Yaroslava Wenner, Christoph Friedburg, Markus N Preising, Wadim Bowl, Walter Sekundo, Erdmuthe Meyer zu Bexten, Knut Stieger, and Birgit Lorenz, "Optical coherence tomography (oct) device independent intraretinal layer segmentation," *Translational Vision Science and Technology*, vol. 3, no. 1, 2014.

[9] Olivier Laligant, Frédéric Truchetet, and Alain Dupasquier, "Edge enhancement by local deconvolution," *Pattern recognition*, vol. 38, no. 5, pp. 661–672, 2005.

[10] M.J. Kirby and R. Miranda, "Circular nodes in neural networks," *Neural Computation*, vol. 8, no. 2, pp. 390–402, 1996.

[11] Håvard Rue and Merrilee A Hurn, "Bayesian object identification," *Biometrika*, vol. 86, no. 3, pp. 649–660, 1999.

[12] A Belghith, C Collet, and J.P Armspach, "A statistical framework for biomarker analysis and hr-mas 2d metabolite identification," in *Computational Surgery and Dual Training*, pp. 89–112. Springer, 2014.

[13] Sasan Moghimi, Hamid Hosseini, Jay Riddle, Gina Yoo Lee, Elena Bitrian, JoAnn Giaconi, Joseph Caprioli, and Kouros Nouri-Mahdavi, "Measurement of optic disc size and rim area with spectral-domain oct and scanning laser ophthalmoscopy," *Investigative ophthalmology & visual science*, vol. 53, no. 8, pp. 4519–4530, 2012.

[14] Alexandre SC Reis, Neil O'Leary, Miriam J Stanfield, Lesya M Shuba, Marcelo T Nicolela, and Balwantray C Chauhan, "Laminar displacement and prelaminar tissue thickness change after glaucoma surgery imaged with optical coherence tomography," *Investigative ophthalmology & visual science*, vol. 53, no. 9, pp. 5819–5826, 2012.

[15] M.A. Kramer, "Nonlinear principal component analysis using autoassociative neural networks," *AIChE journal*, vol. 37, no. 2, pp. 233–243, 1991.

[16] T. Stamkopoulos, K. Diamantaras, N. Maglaveras, and M. Strintzis, "Ecg analysis using nonlinear pca neural networks for ischemia detection," *Signal Processing, IEEE Transactions on*, vol. 46, no. 11, pp. 3058–3067, 1998.

[17] M. Scholz, F. Kaplan, C.L. Guy, J. Kopka, and J. Selbig, "Non-linear pca: a missing data approach," *Bioinformatics*, vol. 21, no. 20, pp. 3887, 2005.

[18] J. Nocedal and S.J. Wright, *Numerical optimization*, Springer verlag, 1999.

[19] S E Fahlman, "An empirical study of learning speed in back-propagation networks," *Training*, vol. 6, no. 4976, pp. 1–19, 1988.

[20] D Bizios, A Heijl, J Leth Hougaard, and B Bengtsson, "Machine learning classifiers for glaucoma diagnosis based on classification of retinal nerve fibre layer thickness parameters measured by stratus oct," *Acta ophthalmologica*, vol. 88, no. 1, pp. 44–52, 2010.

[21] Phillip Good, *A Practitioner's Guide to Resampling for Data Analysis, Data Mining, and Modeling*, Chapman & Hall/CRC, 2011.